Article

DFT Investigation of H Activation by [M(NHP*n*Pr)('S3')] (M = Ni, Pd). Insight into Key Factors Relevant to the Design of Hydrogenase Functional Models

Giuseppe Zampella, Maurizio Bruschi, Piercarlo Fantucci, and Luca De Gioia

J. Am. Chem. Soc., **2005**, 127 (38), 13180-13189• DOI: 10.1021/ja0508424 • Publication Date (Web): 01 September 2005

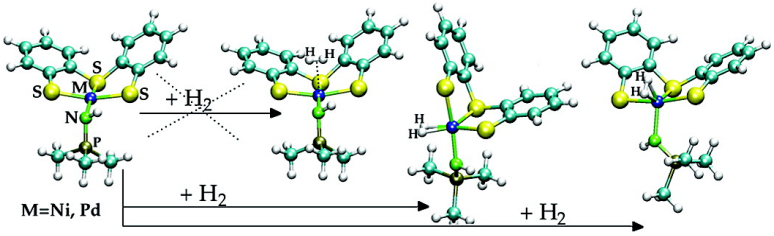

More About This Article

Additional resources and features associated with this article are available within the HTML version:

- Supporting Information
- Links to the 10 articles that cite this article, as of the time of this article download
- Access to high resolution figures
- Links to articles and content related to this article
- Copyright permission to reproduce figures and/or text from this article

View the Full Text HTML

J|A|C|S
ARTICLES
Published on Web 09/01/2005

DFT Investigation of H_2 Activation by [M(NHP*n*Pr$_3$)(′S3′)] (M = Ni, Pd). Insight into Key Factors Relevant to the Design of Hydrogenase Functional Models

Giuseppe Zampella,[†] Maurizio Bruschi,[‡] Piercarlo Fantucci,[†] and Luca De Gioia*[,†]

Contribution from the Department of Biotechnology and Biosciences and Department of Environmental Sciences, University of Milan-Bicocca, Piazza della Scienza 2, I-20156 Milan, Italy

Received February 9, 2005; E-mail: luca.degioia@unimib.it

Abstract: Density functional theory has been used to investigate the reaction between H_2 and [Ni(NHP*n*Pr$_3$)(′S3′)] or [Pd(NHP*n*Pr$_3$)(′S3′)], where ′S3′ = bis(2-sulfanylphenyl)sulfide(2−), which are among the few synthetic complexes featuring a metal coordination environment similar to that observed in the [NiFe] hydrogenase active site and capable of catalyzing H_2 heterolytic cleavage. Results allowed us to unravel the reaction mechanism, which is consistent with an oxidative addition−hydrogen migration pathway for [Ni(NHP*n*Pr$_3$)(′S3′)], whereas metathesis is also possible with [Pd(NHP*n*Pr$_3$)(′S3′)]. Unexpectedly, H_2 binding and activation implies structural reorganization of the metal coordination environment. It turns out that the structural rearrangement in [Ni(NHP*n*Pr$_3$)(′S3′)] and [Pd(NHP*n*Pr$_3$)(′S3′)] can take place due to the peculiar structural features of the Ni and Pd ligands, explaining the remarkable catalytic properties. However, the structural reorganization is the most unfavorable step along the H_2 cleavage pathway ($\Delta G > 100$ kJ mol^{-1}), an observation that is relevant for the design and synthesis of novel biomimetic catalysts.

Introduction

[NiFe] hydrogenases are enzymes that catalyze the reversible oxidation of dihydrogen.[1] In their active site, one Ni ion and one Fe ion are bridged by two cysteine residues; two other cysteines bind the Ni ion, and the coordination environment of Fe is completed by two CN^- ligands and one CO ligand.[2] [NiFe] hydrogenases have been extensively studied using several experimental[3] and theoretical[4] approaches, which led to the characterization of key intermediate species involved in the catalytic cycle. However, some relevant issues, such as the site of H_2 binding and activation, the redox state of Ni during the cleavage step, as well as the nature of the base group involved in the reaction, are still controversial.[5]

The investigation of structural and functional synthetic models of enzymes active sites can nicely complement enzymatic studies and highlight key structural and electronic features relevant to understand the catalytic properties of metal containing cofactors.[6] In the specific context of hydrogenase models, the design and synthesis of coordination compounds characterized by catalytic properties pertinent to hydrogen production is relevant also for energy transduction technology.[7] In fact, the investiga-

[†] Department of Biotechnology and Biosciences.
[‡] Department of Environmental Sciences.

(1) Albracht, S. P. *Biochim. Biophys. Acta* **1994**, *1188*, 167. Graf, E. G.; Thauer, R. K. *FEBS Lett.* **1981**, *136*, 165. Adams, M. W. W. *Biochim. Biophys. Acta* **1990**, *1020*, 115. Cammack, R., Frey, M., Robson, R., Eds. *Hydrogen as fuel − Learning from Nature*; Taylor and Francis: London, 2001.
(2) Volbeda, A.; Charon, M. H.; Piras, C.; Hatchikian, E. C.; Frey, M.; Fontecilla-Camps, J. C. *Nature* **1995**, *373*, 580. Volbeda, A.; Garcin, E.; Pieras, C.; De Lacey, A. L.; Fernandez, V. M.; Hatchikian, E. C.; Frey, M.; Fontecilla-Camps, J. C. *J. Am. Chem. Soc.* **1996**, *118*, 12989. Garcin, E.; Vernede, X.; Hatchikian, E. C.; Volbeda, A.; Frey, M.; Fontecilla-Camps, J. C. *Structure* **1999**, *7*, 557. Higuchi, Y.; Yagi, T.; Yasuoka, N. *Structure* **1997**, *5*, 1671. Higuchi, Y.; Ogata, H.; Miki, K.; Yasuoka, N.; Yagi, T. *Structure* **1999**, *7*, 549. Ogata, H.; Mizoguchi, Y.; Mizuno, N.; Miki, K.; Adachi, S.; Yasuoka, N.; Yagi, T.; Yamauchi, O.; Hirota, S.; Higuchi, Y. *J. Am. Chem. Soc.* **2002**, *124*, 11628.
(3) Cammack, R. *Nature* **1999**, *397*, 214. Nicolet, Y.; Lemon, B. J.; Fontecilla-Camps, J. C.; Peters, J. W. *Trends Biochem. Sci.* **2000**, *25*, 138. Peters, J. W. *Curr. Opin. Struct. Biol.* **1999**, *9*, 670. Horner, D. S.; Heil, B.; Happe, T.; Embley, T. M. *Trends Biochem. Sci.* **2002**, *27*, 148. Nicolet, Y.; Cavazza, C.; Fontecilla-Camps, J. C. *J. Inorg. Biochem.* **2002**, *91*, 1. Fernandez, V. M.; Hatchikian, E. C.; Cammack, R. *Biochim. Biophys. Acta* **1985**, *832*, 69. Teixeira, M.; Mora, I.; Fauque, G.; Czechowski, M.; Berlier, Y.; Lespinat, P. A.; LeGall, J.; Xavier, A. V.; Moura, J. J. G. *Biochimie* **1986**, *68*, 75. Roberts, L. M.; Lindahl, P. A. *Biochemistry* **1994**, *33*, 14339. de Lacey, A. L.; Hatchikian, E. C.; Volbeda, A.; Frey, M.; Fontecilla-Camps, J. C.; Fernandez, V. M. *J. Am. Chem. Soc.* **1997**, *119*, 7181. de Lacey, A. L.; Stadler, C.; Fernandez, V. M.; Hatchikian, E. C.; Fan, H.-J.; Li, S.; Hall, M. B. *J. Biol. Inorg. Chem.* **2002**, *7*, 318. Volbeda, A.; Fontecilla-Camps, J.-C. *J. Chem. Soc., Dalton Trans.* **2003**, 4030. Jones, A. K.; Lamle, S. E.; Pershad, H. R.; Vincent, K. A.; Albracht, S. P. J.; Armstrong, F. A. *J. Am. Chem. Soc.* **2003**, *125*, 8505. De Lacey, A. L.; Fernandez, V. M.; Rousset, M.; Cavazza, C.; Hatchikian, E. C. *J. Biol. Inorg. Chem.* **2003**, *8*, 129. Leger, C.; Dementin, S.; Bertand, P.; Rousset, M.; Guigliarelli, B. *J. Am. Chem. Soc.* **2004**, *126*, 12162. Kurkin, S.; George, S. J.; Thorneley, R. N. F.; Albracht, S. P. J. *Biochemistry* **2004**, *43*, 6820. Foerster, S.; Stein, M.; Brecht, M.; Ogata, H.; Higuchi, Y.; Lubitz, W. *J. Am. Chem. Soc.* **2003**, *125*, 83. Foerster, S.; van Gastel, M.; Brecht, M.; Lubitz, W. *J. Biol. Inorg. Chem.* **2005**, *10*, 51.
(4) Siegbahn, P. E. M.; Blomberg, M. R. A.; Wirstam Pavlov, M.; Crabtree, R. H. *J. Biol. Inorg. Chem.* **2001**, *6*, 460. Fan, H.-J.; Hall, M. B. *J. Biol. Inorg. Chem.* **2001**, *6*, 467. Stein, M.; Lubitz, W. *Curr. Opin. Chem. Biol.* **2002**, *6*, 243. Stein, M.; Lubitz, W. *J. Inorg. Biochem.* **2004**, *98*, 862. Niu, S.; Hall, M. B. *Inorg. Chem.* **2001**, *40*, 6201. Niu, S.; Thomson, L. M.; Hall, M. B. *J. Am. Chem. Soc.* **1999**, *121*, 4000. Fan, H.-J.; Hall, M. B. *J. Am. Chem. Soc.* **2002**, *124*, 394. Stadler, C.; de Lacey, A. L.; Montet, Y.; Volbeda, A.; Fontecilla-Camps, J. C.; Conesa, J. C.; Fernandez, V. M.; *Inorg. Chem.* **2002**, *41*, 4424. Bruschi, M.; De Gioia, L.; Zampella, G.; Reiher, M.; Fantucci, P.; Stein, M. *J. Biol. Inorg. Chem.* **2004**, *9*, 873. Stein, M.; van Lenthe, E.; Baerends, E. J.; Lubitz, W. *J. Am. Chem. Soc.* **2001**, *123*, 5839. Stein, M.; Lubitz, W. *Phys. Chem. Chem. Phys.* **2001**, *3*, 5115. Stein, M.; Lubitz, W. *Phys. Chem. Chem. Phys.* **2001**, *3*, 2668. De Gioia, L.; Fantucci, P.; Guigliarelli, B.; Bertrand, P. *Inorg. Chem.* **1999**, *38*, 2658. De Gioia, L.; Fantucci, P.; Guigliarelli, B.; Bertrand, P. *Int. J. Quantum Chem.* **1999**, *73*, 187.
(5) Armstrong, F. A. *Curr. Opin. Chem. Biol.* **2004**, *8*, 133.

10.1021/ja0508424 CCC: $30.25

tion of the catalytic properties of coordination compounds characterized by sulfur-rich environment has allowed for the disclosure of many aspects relevant to the design of efficient catalysts for H_2 conversion.[8] In particular, several examples of structural models of the [NiFe] hydrogenase active site have been reported.[9] However, nickel complexes featuring hydrogenase-like activity are rare. Catalysis of H_2/D^+ exchange was observed with the thiosemicarbazone complex $[NiL_2]Cl_2$ (L = *o*-C_6H_4(OH)−CN═N−NHCSNH_2),[10] and more recently DuBois and collaborators have reported the synthesis and characterization of the complex $[Ni(Et_2PCH_2NMeCH_2PEt_2)_2]^{2+}$, which incorporates both hydride and proton acceptor sites.[11] Model complexes featuring Ni thiolate cores similar to that observed in the active site of [NiFe] hydrogenases and capable of catalyzing H_2 heterolysis have remained unknown until Sellmann et al.[12] reported the synthesis and catalytic activity of the complex [M(NHP*n*Pr$_3$)(′S3′)], where ′S3′ = bis(2-sulfanylphenyl)sulfide(2−) and M = Ni(II), Pd(II), Pt(II). The D_2/H^+ exchange reaction takes place in 80−120 h under an elevated pressure of D_2 (18 bar) when M = Ni(II).[13] Remarkably, the Ni−Fe complex [(′S_2′Ni−μ(′S_3′)Fe(CO)PMe_3)$_2$] (′S_2′$^{2-}$ = 1,2 benzenedithiolate(2−)), which is characterized by a sulfur-rich square planar nickel coordination environment, is catalytically inactive.[14] Very recently, the Sellmann group has also reported the synthesis and characterization of a trinuclear NiFe cluster that shows structural and functional properties related to [NiFe] hydrogenases.[15]

The dissection of the reaction pathway leading to dihydrogen cleavage, as well as the characterization of intermediate species, can unravel key factors affecting the reactivity, which in turn might facilitate the design of potential catalysts and indirectly shed light on the process of dihydrogen activation taking place in [NiFe] hydrogenase. However, the experimental characterization of short-lived intermediates can be problematic, hindering the full disclosure of the intimate mechanism. In fact, experimental data for [Ni(NHP*n*Pr$_3$)(′S3′)] are consistent with a catalytic cycle that implies interaction of H_2 with the metal center and subsequent cleavage due to the concerted action of the Lewis acid metal ion and one Bronsted basic thiolate donor (Scheme 1).[12]

Scheme 1. Mechanism of D_2/H^+ Exchange Catalyzed by [Ni(NHP*n*Pr$_3$)(′S3′)], As Proposed on the Basis of Experimental Data[12]

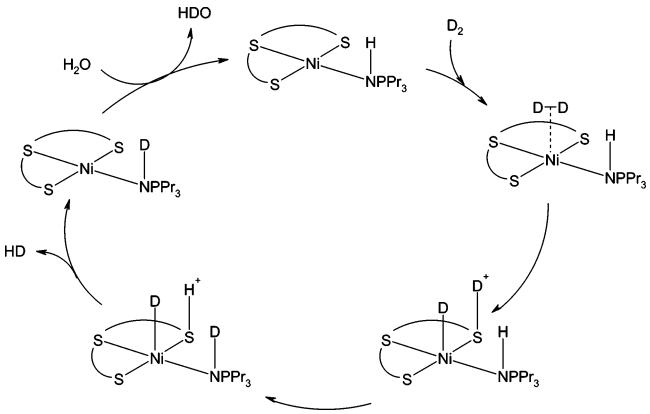

In particular, it has been suggested that the catalytic activity of [Ni(NHP*n*Pr$_3$)(′S3′)] could be due to the strongly flattened tetrahedral geometry of the Ni ion.[12] However, intermediate species have not yet been experimentally characterized, and therefore the key features responsible for catalysis, as well as the mechanism for H_2 activation, are still unknown.

In this contribution, density functional theory has been used to investigate the reaction between H_2 and [Ni(NHP*n*Pr$_3$)(′S3′)] and its Pd analogue, with the aim of characterizing transition states and intermediate species in the pathway leading to H_2 cleavage, and consequently clarifying some of the key factors responsible for its remarkable catalytic activity.

In the first section of the paper, data relative to the tuning of the computational approach to accurately reproduce the structural features of the investigated complexes are presented. Structure, electronic properties, and relative stabilities of intermediate and transition state species obtained investigating different reaction paths leading to H_2 cleavage are discussed in the second section of the paper. Finally, key factors responsible for catalysis, as well as observations relevant to the design of novel efficient catalysts, are discussed.

Methods

DFT calculations have been carried out using both the hybrid functional B3LYP[16] and the pure functional BP86,[17] in conjunction with a valence triple-ζ basis set with polarization on all atoms (TZVP).[18]

The TZVP basis set for Pd is characterized by the contraction scheme [7s6p5d]/[5s3p3d]; the inner electronic core (28 electrons) is treated with the quasi-relativistic Wood−Boring Stuttgart (ECP28MWB) pseudopotential.[19]

Stationary points of the energy hypersurface have been located by means of energy gradient techniques, and full vibrational analysis has been carried out to further characterize each stationary point.

(6) Holm, R. H., Solomon, E. L., Eds. *Chem. Rev.* **2004**, *104*, 347 and articles therein.
(7) Evans, D. J.; Pickett, C. J. *Chem. Soc. Rev.* **2003**, *32*, 268.
(8) Georgakaki, I. P.; Miller, M. L.; Darensbourg, M. Y. *Inorg. Chem.* **2003**, *42*, 2489. Darensbourg, M. Y.; Lyon, E. J.; Smee, J. J. *Coord. Chem. Rev.* **2000**, *206*−*207*, 533. Zhao, X.; Georgakaki, I. P.; Miller, M. L.; Yarbrouch, J. C.; Darensbourg, M. Y. *J. Am. Chem. Soc.* **2001**, *123*, 9710. Gloaguen, F.; Lawrence, J. D.; Rauchfuss, T. B.; Bénard M.; Rohmer M.-M. *Inorg. Chem.* **2002**, *41*, 6573. Boyke, C. A.; Rauchfuss, T. B.; Wilson, S. R.; Rohmer, M.-M.; Benard, M. *J. Am. Chem. Soc.* **2004**, *126*, 15151. Rauchfuss, T. B. *Inorg. Chem.* **2004**, *43*, 14. Evans, D. J.; Pickett, C. J. *Chem. Soc. Rev.* **2003**, *32*, 268. Razavet, M.; Davies, S. C.; Hughes, D. L.; Barclay, J. E.; Evans, D. J.; Fairhurst, S. A.; Liu, X.; Pickett, C. J. *J. Chem. Soc, Dalton Trans.* **2003**, 586. Borg, S. J.; Behrsing, T.; Best, S. P.; Razavet, M.; Liu, X.; Pickett, C. J. *J. Am. Chem. Soc.* **2004**, *126*, 16988. Song, L.-C.; Yang, Z.-Y.; Bian, H.-Z.; Hu, Q.-M. *Organometallics* **2004**, *23*, 3082. Lee, C.-M.; Chen, C.-H.; Ke, S.-C.; Lee, G. H.; Liaw, W.-F. *J. Am. Chem. Soc.* **2004**, *126*, 8406.
(9) Darensbourg, M. Y.; Lyon, E. J.; Smee, J. J. *Coord. Chem. Rev.* **2000**, *206*−*207*, 533. Osterloh, F.; Saak, W.; Hasse, D.; Pohl, S. *Chem. Commun.* **1997**, 979. Davies, S. C.; Evans, D. J.; Hughes, D. L.; Longhurst, S.; Sanders, J. R. *Chem. Commun.* **1999**, 1935. Smith, M. C.; Barclay, J. E.; Cramer, S. P.; Davies, S. C.; Gu, W.-W.; Hughes, D. L.; Longhurst, S.; Evans, D. J. *J. Chem. Soc., Dalton Trans.* **2002**, 2641. Marr, A. C.; Spencer, D. J. E.; Schroder, M. *Coord. Chem. Rev.* **2000**, *206*−*207*, 1055.
(10) Zimmer, M.; Schulte, G.; Luo, X.-L.; Crabtree, R. H. *Angew. Chem., Int. Ed. Engl.* **1991**, *30*, 193.
(11) Curtis, C. J.; Miedaner, A.; Ciancanelli, R.; Ellis, W. W.; Noll, B. C.; Rakowski DuBois, M.; DuBois, D. L. *Inorg. Chem.* **2003**, *42*, 216.
(12) Sellmann, D.; Geipel, F.; Moll, M. *Angew. Chem., Int. Ed.* **2000**, *39*, 561.
(13) Sellmann, D.; Prakash, R.; Heinemann, F. W. *Eur. J. Inorg. Chem.* **2004**, 1847.
(14) Sellmann, D.; Geipel, F.; Lauderbach, F.; Heinemann, F. W, *Angew. Chem., Int. Ed.* **2002**, *41*, 632.
(15) Sellmann, D.; Lauderbach, F.; Geipel, F.; Heinemann, F. W.; Moll, M. *Angew. Chem., Int. Ed.* **2004**, *43*, 3141.
(16) Becke, A. D. *J. Chem. Phys.* **1992**, *96*, 2155. Becke, A. D. *J. Chem. Phys.* **1993**, *98*, 5648. Stevens, P. J.; Devlin, F. J.; Chablowski, C. F.; Frisch, M. J. *J. Phys. Chem.* **1994**, *98*, 11623. Lee, C.; Yang, W.; Parr, R. G. *Phys. Rev.* **1988**, *B37*, 785.
(17) Becke, A. D. *Phys. Rev. A* **1988**, *38*, 3098. Perdew, J. P. *Phys. Rev. B* **1986**, *33*, 8822.
(18) Schafer, A.; Huber, C.; Ahlrichs, R. *J. Chem. Phys.* **1994**, *100*, 5829.
(19) Schwerdtfeger, P.; Dolg, M.; Schwarz, W. H. E.; Bowmaker, G. A.; Boyd, V. *J. Chem. Phys.* **1989**, *91*, 1762. Bergner, A.; Dolg, M.; Kuechle, W.; Stoll, H.; Preuss, H. *Mol. Phys.* **1993**, *80*, 1431.

Table 1. Comparison of Experimental and Theoretical Bond Distances (in Å) and Bond Angles (in deg)[a]

	[Ni(NHP*n*Pr$_3$)('S3')] (X-ray)[28]	[Ni(NHPMe$_3$)('S3')] BP86/TZVP	[Ni(NHPMe$_3$)('S3')] B3LYP/TZVP	[Pd(NHP*n*Pr$_3$)('S3')] (X-ray)[28]	[Pd(NHPMe$_3$)('S3')] BP86/TZVP	[Pd(NHPMe$_3$)('S3')] B3LYP/TZVP
M−S1	2.174	2.222	2.249	2.295	2.372	2.400
M−S2	2.116	2.127	2.179	2.217	2.263	2.322
M−S3	2.184	2.196	2.220	2.305	2.341	2.373
M−N	1.917	1.949	1.952	2.063	2.109	2.050
N−M−S2	170.9	170.1	171.8	175.3	165.8	175.0
S1−M−S3	161.8	162.9	165.7	163.5	176.4	162.5

[a] Atoms are labeled according to Figure 1. M is either Ni or Pd.

The optimization of transition state structures has been carried out according to a procedure based on a pseudo Newton−Raphson method. Initially, geometry optimization of a guessed transition state structure is carried out constraining the distance corresponding to the reaction coordinate. Vibrational analysis at BP86/TZVP level of the constrained minimum energy structures is then carried out, and, if one negative eigenmode corresponding to the reaction coordinate is found, the curvature determined at such point is used as a starting point in the transition state search. The location of the transition state structure is carried out using an eigenvector-following search: the eigenvectors in the Hessian are sorted in ascending order, the first one being that associated with the negative eigenvalue. After the first step, however, the search is performed by choosing the critical eigenvector with a maximum overlap criterion, which is based on the dot product with the eigenvector followed at the previous step.

The charge distributions of the complexes were analyzed by standard Mulliken analysis[20] and by the Roby−Davidson methods,[21] which has been shown to be well suited to describe coordination compounds.[22] Calculations have been carried out with the TURBOMOLE 5.1 suite[23] applying the resolution-of-the-identity technique[24] for BP86/TZVP calculations.

Free energy (G) values have been obtained from the electronic SCF energy considering three contributions to the total partition function (Q), $q_{translational}$, $q_{rotational}$, $q_{vibrational}$, under the assumption that Q may be written as the product of such terms.[25] To evaluate enthalpy and entropy contributions, the values for temperature, pressure, and scaling factor for the SCF wavenumbers have been set to 298.15 K, 18 bar, and 0.9, respectively. Rotations have been treated classically, and vibrational modes have been described according to the harmonic approximation.

Solvation effects (CH_2Cl_2; $\epsilon = 8.94$), which have been evaluated according to the COSMO approach,[26] turned out to affect relative energy differences by less than 2 kJ mol^{-1}.

Even though experimental evidence for the formation of high-spin species in the enzyme catalytic cycle has been recently obtained,[27] the possible formation of high-spin Ni(II) species has not been studied because NMR spectra of the complexes investigated in the present contribution are consistent only with low-spin species.[13]

Results

Evaluation of the Computational Protocol. Initially, with the aim of verifying the accuracy of the adopted DFT approach in reproducing the structural features of the parent complex [Ni(NHP*n*Pr$_3$)('S$_3$')], we have optimized, using both hybrid (B3LYP) and pure (BP86) functionals, the model [Ni(NHPMe$_3$)('S$_3$')], which differs from [Ni(NHP*n*Pr$_3$)('S$_3$')] only for the replacement of the propyl chains bound to the phosphorus center with methyl groups. Both B3LYP/TZVP and BP86/TZVP led to optimized structures that fit well with the X-ray data (Table 1).[28]

Importantly, the peculiar strongly flattened tetrahedral coordination geometry observed in [Ni(NHP*n*Pr$_3$)('S$_3$')] is very well reproduced by both functionals. However, B3LYP/TZVP calculations resulted in a systematic overestimation, by about 0.05 Å, of Ni−S bond lengths. On the other hand, corresponding bond distances obtained with the BP86 functional are affected by smaller deviations with respect to experimental data (Table 1). Similar considerations hold true for the homologue Pd model [Pd(NHPMe$_3$)('S$_3$')] (Table 1), in line with previous data indicating that the BP86 functional is well suited to reproduce accurately the structural features of Ni complexes in sulfur-rich coordination environments.[4]

To complete the computational characterization of [Ni(NHPMe$_3$)('S$_3$')], we have carried out also geometry optimization of structures where the NHPMe$_3$ group is rotated along the Ni−N axis with respect to the X-ray structure of [Ni(NHP*n*Pr$_3$)('S$_3$')]. This search led to the characterization of two conformers differing for the value of the dihedral angle H−N−Ni−S3 (−131° and 37°). The coordination geometry of the Ni center is unaffected by Ni−N bond rotation (data not shown), and the two conformers differ in energy by less than 2 kJ mol^{-1}, indicating, in agreement with experimental results,[13] that these species can coexist at room temperature. Similar results have been obtained for the homologue Pd complex (data not shown).

Reactivity of [Ni(NHPMe$_3$)('S$_3$')] and [Pd(NHPMe$_3$)('S$_3$')]. Once it was verified that the BP86/TZVP level of theory allows the accurate reproduction of the structural features of the parent model [Ni(NHPMe$_3$)('S$_3$')] (hereafter referred to as **1**; Figure 1), we turned our attention to the investigation of its reactivity properties.

Sellmann and collaborators suggested that the first species formed upon reaction of [Ni(NHP*n*Pr$_3$)('S$_3$')] with H_2 could be a transient adduct where dihydrogen is coordinated to the Ni ion in a nonclassical way (Scheme 2).[12] However, geometry optimization of square pyramidal adducts between **1** and H_2, in which the NHPMe$_3$ group and H_2 occupy equatorial and axial positions, respectively, does not correspond to stable species and results in H_2 dissociation from the complex. Remarkably, adducts between H_2 and **1** correspond to stable intermediate species only when the Ni center assumes a distorted square pyramidal geometry featuring sulfur atoms and dihydrogen in

(20) Mulliken, R. S. *J. Chem. Phys.* **1955**, *23*, 1833.
(21) Davidson, E. R. *J. Chem. Phys.* **1967**, *46*, 3320. Roby, K. R. *Mol. Phys.* **1974**, *27*, 81. Heinzmann, R.; Ahlrichs, R. *Theor. Chim. Acta* **1976**, *42*, 33.
(22) Mylvaganam, K.; Bacskay, G. B.; Hush, N. S. *J. Am. Chem. Soc.* **2000**, *122*, 2041.
(23) Ahlrichs, R.; Bar, M.; Haser, M.; Horn, H.; Kolmel, C. *Chem. Phys. Lett.* **1989**, *162*, 165.
(24) Eichkorn, K.; Weigend, F.; Treutler, O.; Ahlrichs, R. *Theor. Chem. Acc.* **1997**, *97*, 119.
(25) Jensen, F. *Introduction to Computational Chemistry*; John Wiley & Sons Ltd.-Baffins Lane: Chichester, England.
(26) Klamt, A. *J. Phys. Chem.* **1995**, *99*, 2224. Klamt, A. *J. Phys. Chem.* **1996**, *100*, 3349.
(27) Wang, H.; Ralston, C. Y.; Patil, D. S.; Jones, R. M.; Gu, W.; Verhagen, M.; Adams, M.; Ge, P.; Riordan, C.; Marganian, C. A.; Mascharak, P.; Kovacs, J.; Miller, C. G.; Collins, T. J.; Brooker, S.; Croucher, P. D.; Wang, K.; Stiefel, E. I.; Cramer, S. P. *J. Am. Chem. Soc.* **2000**, *122*, 10544.
(28) Sellmann, D.; Geipel, F.; Heinemann, F. W. *Eur. J. Inorg. Chem.* **2000**, 59.

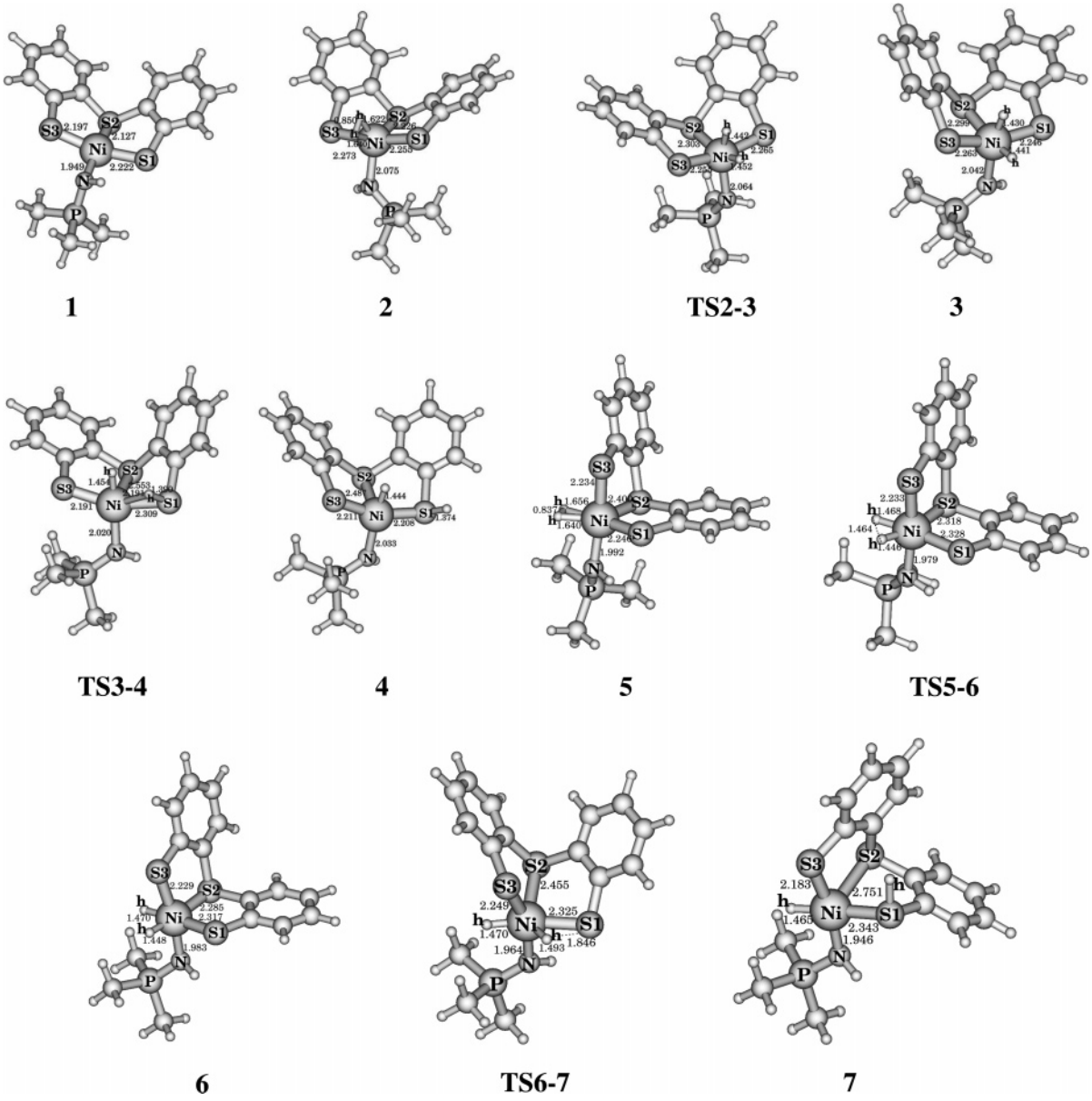

Figure 1. BP86/TZVP optimized structures of intermediate species and transition states for the activation of H_2 catalyzed by [Ni(NHPMe$_3$)(′S3′)].

Scheme 2. Schematic Representation of the Possible H_2 Activation Pathways Promoted by Coordination Compounds

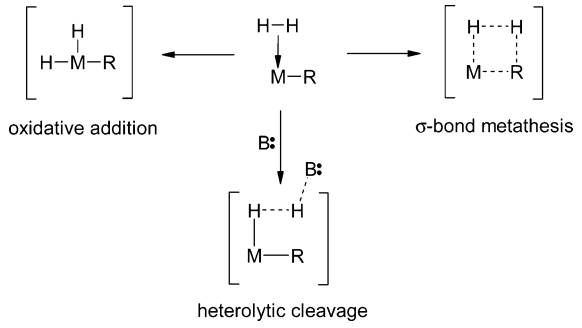

the equatorial plane (**2**; Figure 1). Therefore, the reaction **1** + H_2 → **2**, which is endoergonic by 106.6 kJ mol^{-1}, is accompanied by a drastic rearrangement of the metal coordination environment. In particular, the NHPMe$_3$ group leaves the square planar position occupied in **1** and moves to the axial position in **2**. The H−H bond is perpendicular to the axis connecting S3 and S1, and the H−H distance (0.85 Å) is indicative of nonclassical coordination of dihydrogen (Figure 1).[29]

To investigate the electronic factors affecting the geometry of the H_2 adduct, we have compared the HOMO and LUMO of **1** with the orbitals computed on the corresponding structure obtained by removal of H_2 from **2** (**1′**, which is characterized by optimum electronic energy computed for the nuclei frozen into the geometry of **2**; see Figure 2).

It turned out that both of the frontier orbitals of complex **1** are not suited to interact with an incoming H_2 molecule approaching the axial position. In particular, the HOMO is mainly localized on the thiolate S ligands (S1 and S3), whereas the LUMO, which has mainly $d_{x^2-y^2}$ character, lies in the plane of the ligands and cannot properly interact with the σ-bond of dihydrogen (not shown). On the other hand, in **1′** the HOMO is strongly localized on Ni (Figure 2), and its orientation is

(29) Kubas, G. J. *Acc. Chem. Res.* **1988**, *21*, 120. Gusev, D. G.; Kuhlman, R. L.; Renkema, K. B.; Eisenstein, O.; Caulton, K. G. *Inorg. Chem.* **1996**, *35*, 6775. Maseras, F.; Lledòs, A.; Costas, M.; Poblet, J. M. *Organometallics* **1996**, *15*, 2947.

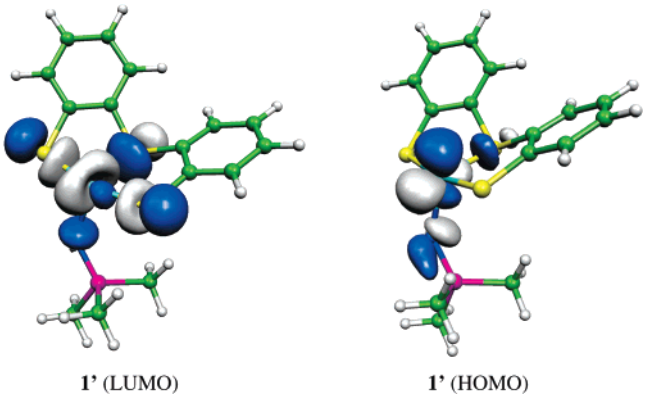

Figure 2. LUMO and HOMO computed for the model complex **1′**, which is obtained from **2** after removal of H_2.

appropriate to interact with the σ^* orbital of the approaching H_2 molecule. Notably, the LUMO in **1′** is only partially localized on the Ni atom, and therefore the interaction between the σ-bond of H_2 and the Ni ion is predicted to be weak. In fact, if the reaction **1** + H_2 → **2** is ideally thought to take place in two steps, **1** → **1′** (reorganization of the Ni coordination environment) followed by **1′** + H_2 → **2** (H_2 binding), it turns out that both steps are endoergonic by 94.9 and 11.7 kJ mol^{-1}, respectively.

To shed light on the mode of H_2 activation by [Ni(NHPMe$_3$)-('S_3')], we have investigated different reaction pathways starting from the precursor **2**. Indeed, it is well known that H_2 activation can be achieved according to either oxidative addition or heterolytic cleavage pathways. In particular, if the system contains an electron-rich metal, homolytic cleavage of the H−H bond can occur via oxidative addition, whereas if the complex contains an electron-deficient metal, which is a poor π-donor, activation of the H−H bond can occur via heterolytic cleavage due to the greatly increased acidity of the H_2 molecule. Indeed, H_2 activation can proceed also through σ-bond metathesis, which implies a four-center transition state and is usually described as homolytic because it does not imply strong polarization, unless the R group is polar, and consequently the distinction between metathesis and heterolytic cleavage becomes fuzzy (Scheme 2). In fact, σ-bond metathesis reactions involving H_2 have gained wide acceptance for complexes of electron-poor transition metals,[30] and both experimental and theoretical evidence[31] indicates that this reaction path can also occur with middle or late transition metal complexes.[32]

The optimized structure of the product of H_2 oxidative addition (**3**) is shown in Figure 1. In **3**, the Ni coordination environment is octahedral and the two H atoms have a cis disposition. The comparison of computed energy values indicates that **3** is less stable than **2** by 9.6 kJ mol^{-1}. To fully characterize this reaction step, we have computed also the transition state structure related to the **2** → **3** conversion (**TS2**−**3**; see Figure 1). In **TS2**−**3**, which has product-like character, as deduced by the large H−H distance (1.357 Å), the Ni center has a distorted octahedral geometry. **TS2**−**3** is less stable than **2** by 19.2 kJ mol^{-1} (Scheme 3).

Comparison of partial charge values computed for **2** and **3** indicates that the term oxidative addition has only a formal meaning in this context. In fact, the partial atomic charge on Ni decreases going from **2** to **3** (see Supporting Information).

As stated above, H_2 might also be cleaved according to σ-bond metathesis or heterolytic cleavage pathways. These reaction pathways imply proton transfer to one sulfide ligand, as observed in the optimized model **4** (Figure 1), where the Ni center has a square pyramidal geometry, the S2 ligand occupies the axial position, and the Ni−S2 distance becomes as long as 2.487 Å. The comparison of computed energy values indicates that the conversion **2** → **4** is endoergonic by 44.7 kJ mol^{-1}. Despite extensive sampling of the potential energy surface, we were not able to locate any transition state along the **2** → **4** pathway, that is, corresponding to H_2 heterolytic cleavage or σ-bond metathesis. Instead, a low-energy transition state was found along the **3** → **4** pathway (**TS3**−**4**). In **TS3**−**4**, one H atom is bridged between Ni and S1, whereas all other structural features are similar to those observed in **3**. Analysis of the normal vibrational mode corresponding to the imaginary frequency reveals that the transition state structure **TS3**−**4** corresponds to migration of one H atom, which moves from the Ni coordination environment to the S1 atom (Figure 1). The computed activation energy associated with **3** → **TS3**−**4** is 54.3 kJ mol^{-1}.

As discussed above, H_2 binding to **1** leads to a significant structural reorganization of the metal center, with the NHPMe$_3$ ligand moving from the equatorial to the axial position. Extensive search for other "nonclassical" H_2 adducts to **1** led to the characterization of another distorted square pyramidal species (**5**) where N, S1, S3, and H_2 occupy the equatorial position, and S2 is the axial ligand (Figure 1). The conversion **1** + H_2 → **5** is endoergonic by 107.8 kJ mol^{-1}. Remarkably, as observed in **2**, also in **5** the binding of H_2 to the metal center is mainly stabilized by back-donation from the Ni HOMO to the σ^* orbital of H_2 (not shown). Consistently with this observation, **5** can undergo oxidative addition, going through the transition state structure **TS5**−**6**, and forming the intermediate octahedral species **6** (Figure 1). Similarly to what was observed for **3**, reductive elimination on **6** leads to **7**, where the Ni coordination environment can be described as a square pyramid where the axial ligand (S2) is loosely bound to nickel (Ni−S2 = 2.751 Å). The structure of the transition state related to the **6** → **7** conversion (**TS6**−**7**) is shown in Figure 1.

The analysis of the energy profile of the **5** → **6** → **7** conversion (Scheme 3) reveals that H_2 cleavage is an endoergonic process characterized by a relatively large activation barrier corresponding to the hydrogen migration step ($\Delta G^{\ddagger}$ = 33.0 kJ mol^{-1}; **6** → **7**). Also, in this case we were not able to find any transition state structure related to σ-bond metathesis or heterolytic cleavage pathways (i.e., **5** → **7** step).

Prompted by the experimental observation that also the complex containing Pd(II) can catalyze H_2 cleavage,[12] we have

(30) Jessop, P. G.; Morris, R. H. *Coord. Chem. Rev.* **1992**, *121*, 155. Crabtree, R. H. *Angew. Chem., Int. Ed. Engl.* **1993**, *32*, 789. Arndtsen, B. A.; Bergman, R. G.; Mobley, T. A.; Peterson, T. H. *Acc. Chem. Res.* **1995**, *28*, 154. Folga, E.; Woo, T.; Ziegler, T. In *Theoretical Aspects of Homogeneous Catalysis*; van Leeuwen, P. W. N. M., Morokuma, K., van Lenthe, J. H., Eds.; Kluwer: Dordrecht, 1995; p 115 and refs therein.
(31) Joshi, A. M.; James, B. R. *Organometallics* **1990**, *9*, 199. Burger, P.; Bergman, R. G. *J. Am. Chem. Soc.* **1993**, *115*, 10462. Lee, J. C.; Peris, E.; Rheingold, E. A. L.; Crabtree, R. H. *J. Am. Chem. Soc.* **1994**, *116*, 11014. Musaev, D. G.; Medel, A. M.; Morokuma, K. *J. Am. Chem. Soc.* **1994**, *116*, 10693. Versluis, L.; Ziegler, T. *Organometallics* **1990**, *9*, 2985. Siegbahn, P. E. M.; Crabtree, R. H. *J. Am. Chem. Soc.* **1996**, *118*, 4442.
(32) Hutschka, F.; Dedieu, A. *J. Chem. Soc., Dalton Trans.* **1997**, 1899.

Scheme 3. Relative Free Energies (in kJ mol^{-1}) Computed for Intermediate Species and Transition States Involved in the Activation of H_2 by [Ni(NHPMe$_3$)('S$_3$')] According to Reaction Paths Involving the Ni−H_2 Intermediate Species **2** (Path a) and **5** (Path b)

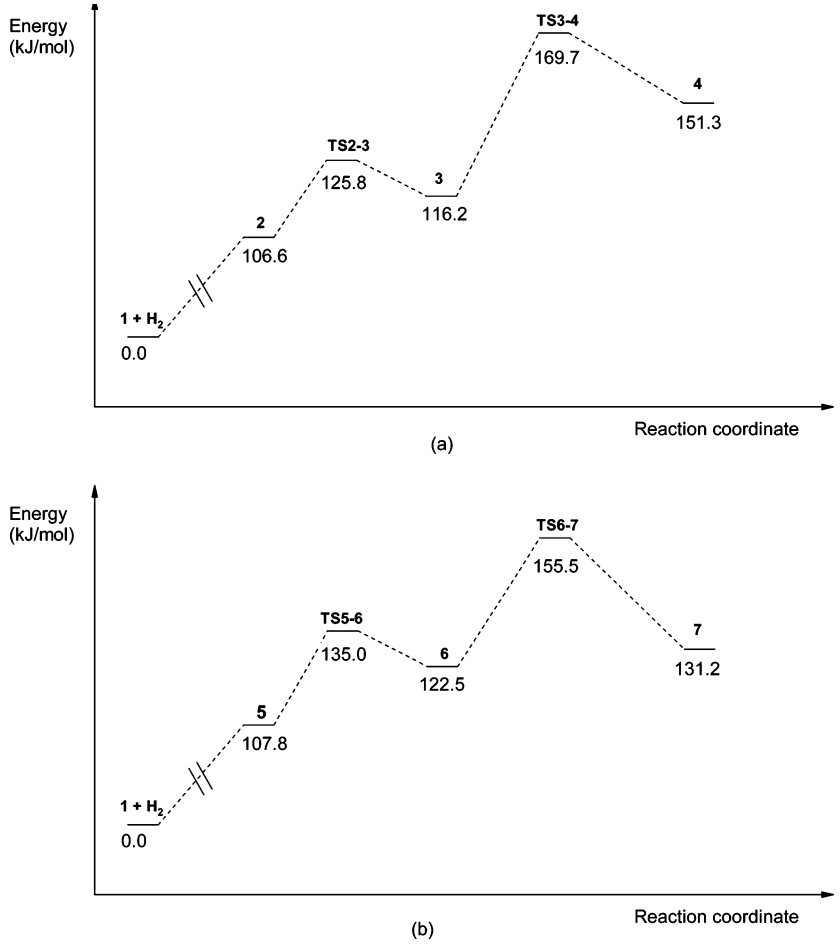

investigated the reaction paths promoted by [Pd(NHPMe$_3$)('S'3)] (hereafter referred to as **8**), whose optimized structure is shown in Figure 3.

The search for a stable adduct between H_2 and **8** led to the characterization of the model complex **9** (Figure 3), where Pd has distorted square pyramidal geometry with N, S1, S3, and H_2 in the equatorial position and S2 in the axial position. The reaction **8** + H_2 → **9** is endoergonic by 122.5 kJ mol^{-1}. As was observed for the corresponding Ni complexes, H_2 coordination is accompanied by structural reorganization of the metal coordination environment. However, the comparison of **9** to the Ni homologue species **2** reveals subtle structural differences in H_2 coordination. While in **2** the NHPMe$_3$ group has axial position and H_2 is in the plane defined by the three S atoms (Figure 1), in **9** H_2 occupies a basal position of the square pyramid. Moreover, in **9** the axial ligand S2 is loosely coordinated to Pd (Pd−S2 distance = 2.780 Å).

The analysis of the HOMO and LUMO computed for **8**, as well as for the structure obtained removing H_2 from **9** (**8′**; Figure 4), reveals that the frontier orbitals in **8** do not have the proper orientation to interact with an incoming H_2 molecule (not shown). On the other hand, and differently from **1′**, the LUMO in **8′** is strongly localized on Pd and is suited to interact with the σ-bond of a H_2 molecule approaching trans to the Pd−N bond (Figure 4). The HOMO is more delocalized and consequently is expected to play a less important role in the H_2−Pd interaction.

Indeed, if also the reaction **8** + H_2 → **9** is ideally dissected in two steps, **8** → **8′** (reorganization of the Pd coordination environment), and **8′** + H_2 → **9** (H_2 binding), it turns out that the first step is endoergonic by 151.3 kJ mol^{-1}, whereas the second step is exoergonic by 28.8 kJ mol^{-1}.

Also, for the H_2−Pd complex **9**, H_2 activation can in principle proceed according to either an oxidative addition or a heterolytic cleavage/metathesis pathway. In **10**, which is the intermediate species formed after H_2 oxidative addition, the Pd atom lies in an octahedral environment, the two H atoms are cis to each other, and the S2−Pd bond has shortened with respect to the precursor **9**. The **9** → **10** step is exoergonic by 8.4 kJ mol^{-1}. The energy barrier along the **9** → **10** pathway (**TS9**−**10**) is 7.5 kJ mol^{-1} (Scheme 4).

As was observed in the homologue Ni species, **10** can undergo hydrogen migration. The corresponding transition state structure (**TS10**−**11**), which is higher in energy than **10** by 42.6 kJ mol^{-1}, is characterized by one H atom bridging Pd and S3. The product derived from H_2 cleavage according to the oxidative addition−hydrogen migration pathway (**11**) is less stable than **9** by 13.8 kJ mol^{-1} and is characterized by a very elongated (2.915 Å) Pd−S2 bond (Figure 3).

H_2 activation on **9** to form **11** can also proceed via a transition state structure (**TS9**−**11**; Figure 3) reminiscent of the classical 4-center transition states reported for σ-bond metathesis.[32,33] In

(33) Niu, S.-Q.; Hall, M. B. *Chem. Rev.* **2000**, *100*, 353.

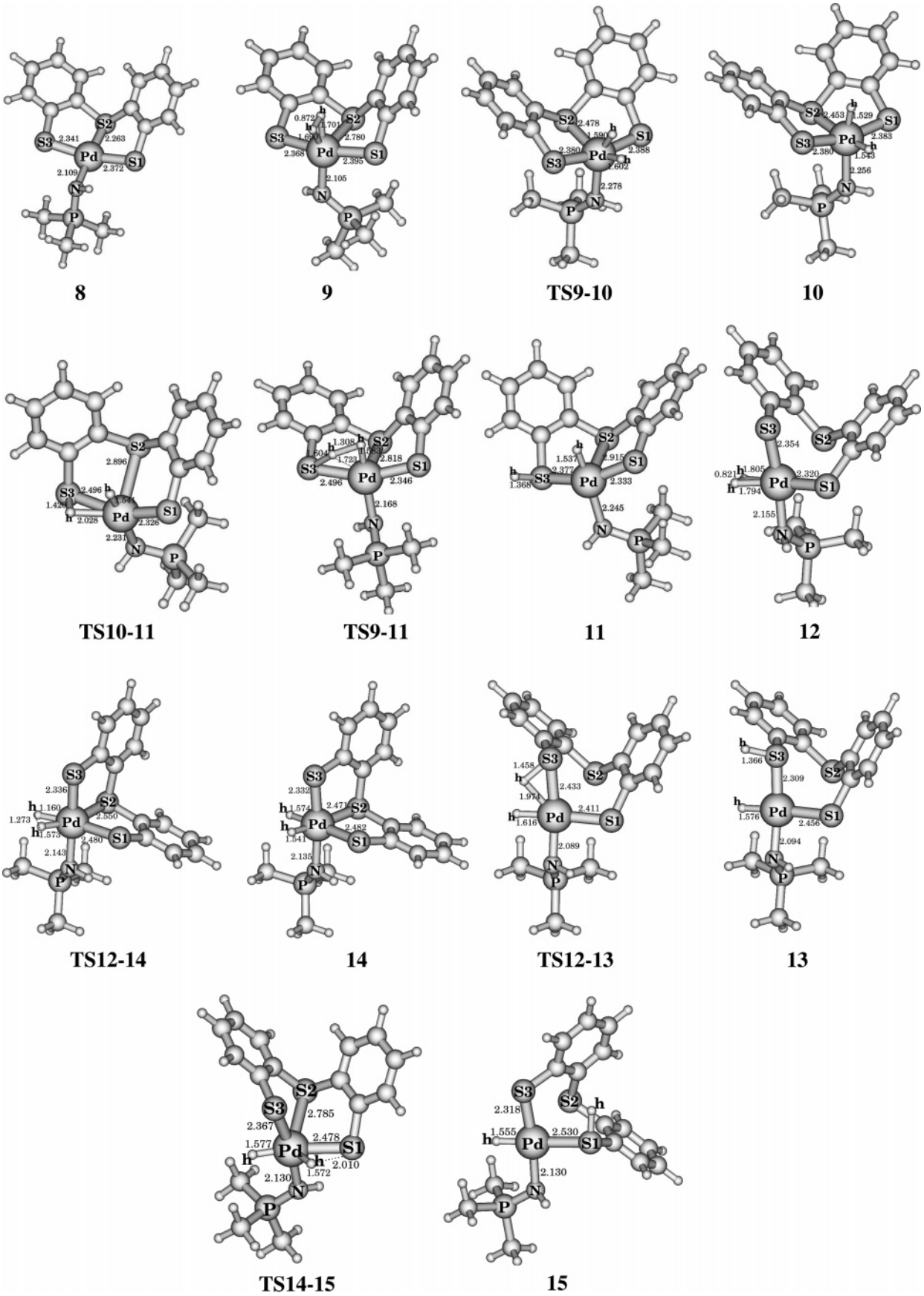

Figure 3. BP86/TZVP optimized structures of intermediate species and transition states for the activation of H_2 catalyzed by [Pd(NHPMe$_3$)(′S3′)].

TS9−11, the H−H distance is 1.308 Å and the H atom transferred to the sulfur center still interacts with the metal ion. The activation energy associated with the **9** → **TS9−11** step is 43.5 kJ mol^{-1} (Scheme 4).

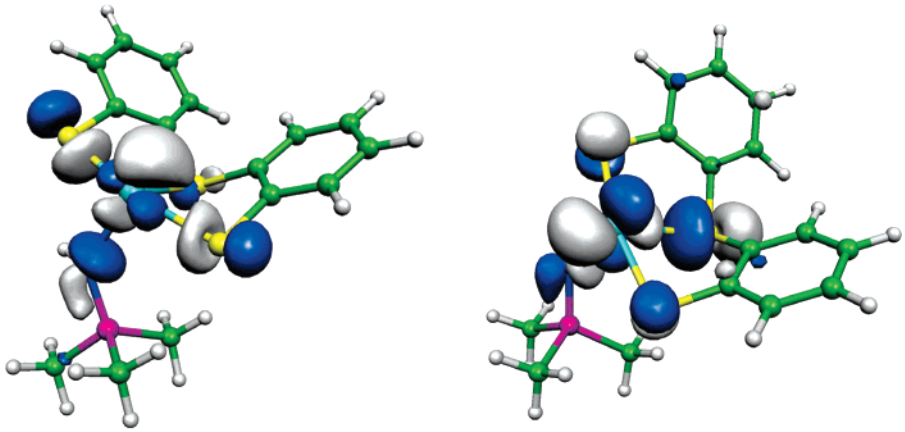

8' (LUMO) 8' (HOMO)

Figure 4. LUMO and HOMO computed for the model complex **8′**, which is obtained from **9** after removal of H_2.

Scheme 4. Relative Free Energies (in kJ mol^{-1}) Computed for Intermediate Species and Transition States Involved in the Activation of H_2 by [Pd(NHPMe$_3$)(′S$_3$′)] According to Reaction Paths Involving the Pd−H_2 Intermediate Species **9** (Path a) and **12** (Path b)

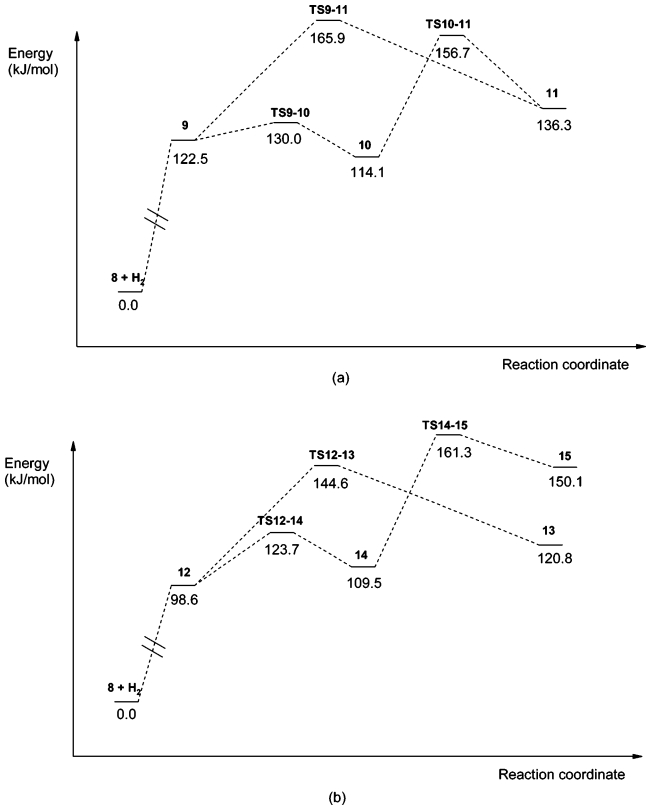

As was observed for the corresponding Ni species, the search for other H_2 "nonclassical" adducts led to the characterization of another isomer (**12**) that can be described as a square pyramid in which the axial Pd−S2 bond is very elongated (2.978 Å; Figure 3). Also, **12** can follow either oxidative addition−hydrogen migration or metathesis pathways. The former pathway goes through the transition state **TS12−14** and leads to the six-coordinated species **14**, which is only slightly less stable than the reactant **12** (ΔG = 10.9 kJ mol^{-1}; Scheme 4). Next, **14** can evolve to **15**, where a H atom has been transferred from Pd to S1. The conversion **14** → **15** is endoergonic by 40.5 kJ mol^{-1} (Scheme 4) and proceeds going through the transition state **TS14−15** (Figure 4), which is 51.8 kJ mol^{-1} higher in energy than **14**. The metathesis pathway goes through the transition state structure **TS12−13** and leads to the square pyramidal species **13**, where one H atom is in the equatorial plane and the axial Pd−S2 bond is very elongated (3.453 Å). The products obtained after H_2 cleavage (**13** and **15**) differ for the protonation site (S3 in **13** and S1 in **15**). Moreover, **13** is more stable than **15** by 29.3 kJ mol^{-1}

Discussion

Even though a discrete number of synthetic complexes resembling the structure of the [NiFe] hydrogenase active site are known,[9] [Ni(NHP*n*Pr$_3$)(′S$_3$′)] remains one of the very few synthetic complexes capable of catalyzing H_2 heterolytic cleavage and featuring a Ni coordination environment similar to the enzyme. However, an elevated pressure of D_2 (18 bar) is necessary to observe the D_2/H^+ exchange reaction, which takes place in 80 h,[13] hindering practical applications in H_2 conversion technology. These observations prompted us to undertake the DFT dissection of the mechanism of H_2 cleavage, with the aim of shedding light on key features for catalysis and possibly highlighting factors responsible for the experimentally observed slow reaction rates.

The first relevant result obtained investigating the interaction between **1** and H_2 is related to the structural and electronic features of the H_2 adducts (**2** and **5**). Formation of a nonclassical H_2 adduct implies a dramatic rearrangement of the Ni coordination environment, with one ligand (N in **2** and S2 in **5**) moving from the equatorial to the axial position. In fact, H_2 cannot bind to the apical position of the square planar parent complex **1**. Therefore, the structural reorganization of the Ni coordination environment is a necessary prerequisite for H_2 binding. It should be noted that, in principle, H_2 activation could not necessarily imply the formation of a nonclassical H_2 intermediate adduct and could proceed via a reaction pathway in which the incoming H_2 molecule evolves directly toward a species where H_2 is cleaved (Scheme 5).

However, square pyramidal complexes characterized by a hydride group in the axial position do not correspond to stable intermediate species (not shown) and spontaneously evolve to **4** or **7** (Figure 1), confirming that the structural reorganization of the Ni coordination environment is a prerequisite for H_2 binding and activation. This observation is relevant in light of

Scheme 5. A Plausible Pathway for H_2 Activation That Does Not Imply the Formation of a Nonclassical H_2 Adduct

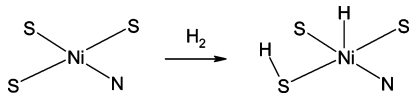

the strongly flattened tetrahedral geometry observed in [Ni(NHP*n*Pr$_3$)(′S$_3$′)][12] and reproduced in its "in silico" model **1**. In fact, the steric demand of the (′S$_3$′) and NHP*n*Pr$_3$ ligands is not compatible with a perfect square planar arrangement, whereas the conversion to a square pyramidal geometry with H_2 in the equatorial plane is possible despite the bulkiness of the chelating (′S$_3$′) group. Hence, the peculiar structural adaptability of [Ni(NHP*n*Pr$_3$)(′S$_3$′)] is proposed to be a key factor in allowing H_2 binding (and consequently activation). Indeed, the formation of the H_2 adduct (**1** + H_2 → **2**, **1** + H_2 → **5**) is the main contribution to the endoergonicity in the H_2 cleavage pathway (Scheme 3). In particular, the dissection of the reaction in reorganization of the Ni coordination environment followed by H_2 binding shows that the endoergonicity can be almost fully ascribed to the first step, an observation that might be relevant for the design of new biomimetic catalysts (see below).

As is well known, the interaction between a coordination compound and the H−H σ-bond is governed by both the extent of π-back-donation from d-orbitals on the metal to the σ^* antibonding H−H orbital and the donation from the H−H σ-bonding orbital to an appropriate empty metal orbital. Notably, both interactions weaken the H−H bond. The former, which plays a predominant role in the Ni−H_2 adducts **2** and **5** (Figures 1 and 2), is expected to favor oxidative addition pathways, whereas the latter, which becomes significant in the Pd−H_2 adducts (**9**, **12**; Figures 3 and 4), increases H_2 acidity and consequently should favor heterolytic cleavage. In agreement with this observation, H_2 activation in **2** and **5** takes place according to an oxidative addition mechanism. In fact, precedent for H_2 oxidative addition to Ni(II) complexes, leading to formal Ni(IV) species, is known.[34] It should be stressed that the Ni(IV) oxidation state has only a formal meaning for the complexes discussed in the present contribution, as deduced by analysis of partial atomic charges (Supporting Information). Accordingly, the H atom bound to Ni has a very small hydride character.

Oxidative addition of H_2 is a facile step, both kinetically and thermodynamically (**2** → **3**, **5** → **6**; Scheme 3). The intermediate species **3** and **6** can further evolve, according to a hydrogen migration step (**3** → **4**, **6** → **7**, Scheme 4), to species that are characterized by an exchangeable acidic proton bound to sulfur. Also, the energy gaps and barriers related to the hydrogen migration step are small when compared to the energy difference associated with the formation of the nonclassical H_2 adduct. It is also interesting to note that the Ni−S2 distance becomes very long in the product of H_2 activation **4** and **7** (Figure 1), suggesting that the S2 ligand could be lost if the ancillary ligand were not tridentate, an observation that can be relevant for the design of new catalysts.

On the ground of the above observations, a refined version of the mechanism of D_2/H^+ exchange catalyzed by [Ni(NHP*n*Pr$_3$)(′S$_3$′)] can be proposed (Scheme 6).

An oxidative addition−hydrogen migration mechanism for H_2 cleavage can be operative also for the corresponding Pd model (**8**). In particular, the formation of the H_2 adducts (**9**,

Scheme 6. Mechanism of D_2/H^+ Exchange Catalyzed by [Ni(NHP*n*Pr$_3$)(′S3′)], As Proposed on the Basis of Experimental[12] and DFT Results

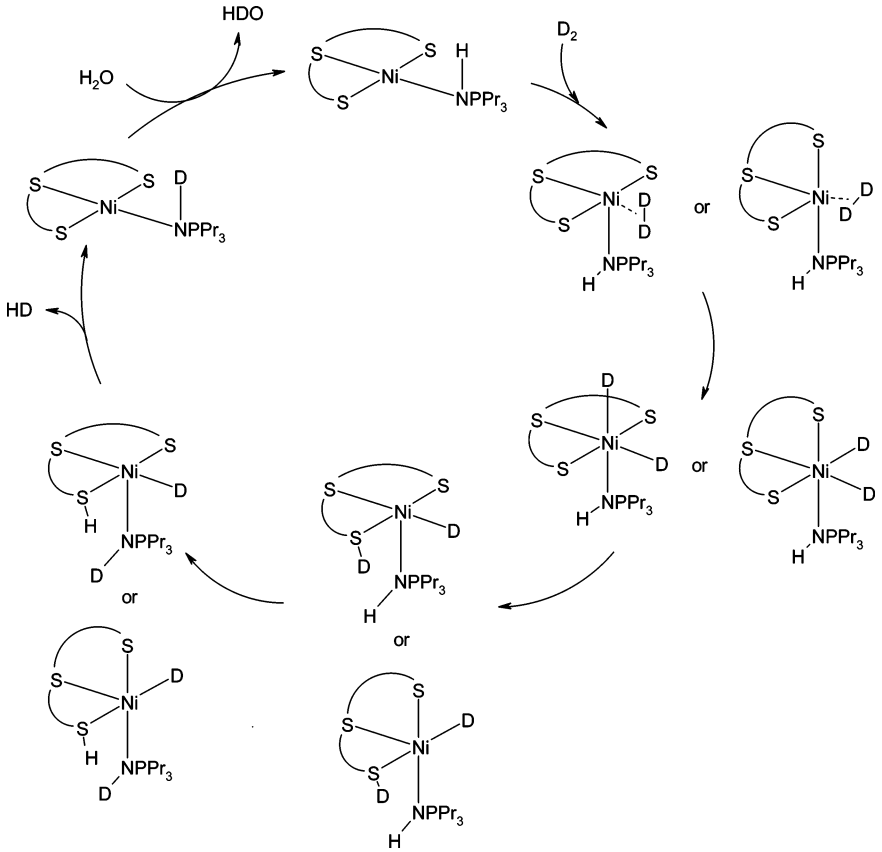

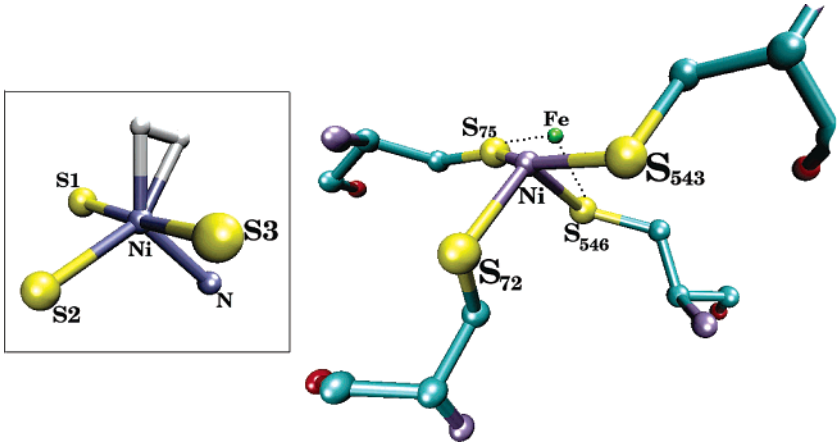

Figure 5. Comparison between the Ni−S_4 coordination environment in [NiFe] hydrogenases[2] and the intermediate species **2** (inlet).[37] The S atoms of the protein are labeled according to the corresponding cysteine residues in the enzyme from *Desulfovibrio fructosovorans*.

12; Figure 3 and Scheme 4) remains the most unfavorable step, while oxidative addition is facile. In fact, dissection of the reaction energy associated with the **8** + H_2 → **9** step leads to the conclusion that reorganization of the Pd coordination environment is very endoergonic, whereas H_2 binding, differently from what was observed for the homologous Ni complex, is exoergonic. The latter observation highlights the different nature of the M−H_2 bond in Ni and Pd complexes, in agreement with the HOMO−LUMO analysis.

As was observed for the corresponding Ni complex, the larger barrier in the oxidative addition−hydrogen migration pathway for H_2 cleavage is associated with the hydrogen migration step (**10** → **11**, **14** → **15**; Scheme 4). However, molecular orbital analysis (Figure 4) suggests an increased acidity of H_2 when coordinated to the Pd complex. In fact, H_2 cleavage on **8** can proceed also according to a σ-bond metathesis pathway going through four-center transition state structures (**TS9**−**11**, **TS12**−**13**; Figure 3). The analysis of computed partial charge values evidences that the activated H_2 moiety is significantly polarized in **TS9**−**11** and **TS12**−**13**, indicating that the H_2 cleavage has heterolytic character (Supporting Information). Remarkably, the computed activation energies for the σ-bond metathesis (**TS9**−**11**, **TS12**−**13**) and for the oxidative addition−hydrogen migration (**TS10**−**11**, **TS14**−**15**) pathways taking place on [Pd(NHPMe$_3$)(′S_3′)] are very similar (Scheme 4), suggesting that the Pd complex **8** can follow both H_2 activation routes. It should be noted that both oxidative addition−hydrogen migration and metathesis pathways lead to products in which H_2 has been cleaved to H^+ and H^-, in agreement with experimental findings indicating that the overall reaction pathway has a heterolytic character.[12] Experiments with *para*-hydrogen, as those recently used to elucidate mechanistic issues related to activation of H_2 over Rh_2S_2 complexes,[35] could clarify some of these aspects.

The structure of intermediate species obtained dissecting the mechanism of H_2 cleavage catalyzed by the Ni complex **1** can be also discussed in light of the structure of the [NiFe] hydrogenase active site.[2] The Ni coordination environment within the enzyme exhibits a large distortion from either an ideal tetrahedral or a square pyramidal geometry.[2,11] In fact, the geometry of the sulfur ligands around the Ni center is very similar in all [NiFe] hydrogenase X-ray structures presently available,[2] and it can be conveniently described as a slightly distorted trigonal bipyramid in which one vertex (ligand) is missing (Figure 5). Remarkably, a very similar arrangement of the ligands is observed in [Ni(NHPMe$_3$)(′S3′)] upon H_2 coordination (**2** and **5**; Figures 1 and 5),[36] indicating that the Ni coordination environment in the enzyme active site may have the proper structural features to allow the formation of Ni−H_2 adducts.

Notably, as discussed above, the rearrangement of the Ni coordination environment in [Ni(NHPMe$_3$)(′S3′)], which is a prerequisite for H_2 binding and activation, is a very endoergonic step (**1** + H_2 → **2**, ΔG = 106.6 kJ mol^{-1}; **1** + H_2 → **5**, ΔG = 107.8 kJ mol^{-1}), in agreement with the experimental observation that D_2/H^+ exchange is not observed under mild conditions.[12] As a consequence, Ni coordination compounds characterized by chelating sulfur ligands, as in the Sellmann complex [Ni(NHPMe$_3$)(′S3′)], but in which the metal coordination environment cannot assume square planar geometry, might have promising catalytic properties for H_2 conversion.

Acknowledgment. This paper is dedicated to the memory of Professor Dieter Sellmann.

Supporting Information Available: Roby−Davidson and Mulliken charges for intermediate species and transition states relevant to the H_2 activation catalyzed by [Ni(NHPMe$_3$)(′S3′)] and [Pd(NHPMe$_3$)(′S3′)]. This material is available free of charge via the Internet at http://pubs.acs.org.

JA0508424

(34) Ayllon, J. A.; Sayers, S. F.; Sabo-Etienne, S.; Donnadieu, B.; Chaudret, B.; Clot, E. *Organometallics* **1999**, *18*, 3981.
(35) Ienco, A.; Calhorda, M. J.; Reinhold, J.; Reineri, F.; Bianchini, C.; Peruzzini, M.; Vizza, F.; Mealli, C. *J. Am. Chem. Soc.* **2004**, *126*, 11954.

(36) Note that in **5** the S1−Ni−S2 angle is smaller (94.3°) than the corresponding angle in **2** (S2−Ni−N = 110.8°) because S1 and S2 are somewhat constrained by the structure of the chelating ligand ′S3′.
(37) The S2−Ni−N angle in **2** is 110.8°. The corresponding angle in **5** (S1−Ni−S2) is 94.3°. In a regular trigonal bipyramid, this angle is 120°. The equivalent angles in the protein (corresponding to S_{72}−Ni−S_{546}) vary in the range 107.7−112.3° in the available X-ray structures, with the exception of 1FRV (91.3°). The S1−Ni−S3 angle in **2** is 169.0°. The corresponding angle in **5** (S3−Ni−N) is 168.1°. In a regular trigonal bipyramid, this angle is 180°. The equivalent angles in the protein (corresponding to S_{75}−Ni−S_{543}) vary in the range 165.8−174.8°, with the exception of 1FRF (157.7°).